RSC Advances

PAPER

View Article Online
View Journal | View Issue

Cite this: *RSC Adv.*, 2020, **10**, 35062

Thermodynamic analysis of dissociation of periodic dislocation dipoles in isotropic crystals

X. W. Zhou

In the past, experimentally observed dislocations were often interpreted using an isolated dislocation assumption because the effect of background dislocation density was difficult to evaluate. Contrarily, dislocations caused by atomistic simulations under periodic boundary conditions can be better interpreted because linear elastic theory has been developed to address the effect of periodic dislocation array in the literature. However, this elastic theory has been developed only for perfect dislocations, but not for dissociated dislocations. The periodic boundary conditions may significantly change the dissociation energy of dislocations and stacking fault width, which in turn, change the deformation phenomena observed in simulations. To enable materials scientists to understand the dislocation behavior under the periodic boundary conditions, we use isotropic elastic theory to analyze the thermodynamics of dissociated periodic dislocations with an arbitrary dislocation character angle. Analytical expressions for force, stacking fault width, and energies are presented in the study. Results obtained from the periodic dislocation array were compared with those obtained from isolated dislocations to shed light on the interpretation of experimentally observed and simulated dislocations.

Received 22nd August 2020
Accepted 2nd September 2020

DOI: 10.1039/d0ra07227c

rsc.li/rsc-advances

1. Introduction

Dislocations observed in microscopic experiments are often interpreted using linear elastic theory without considering dislocation–dislocation interactions. Analogously, atomistic simulations often require periodic boundary conditions where any individual dislocation could be imaged into an infinite dislocation array. The linear elastic theory of dislocation array can be used to address the effect of periodic boundary conditions. One successful example is the calculation of dislocation core energies by fitting the linear elastic expression into atomistic simulation data based on an isotropic assumption.[1–6] These studies suggested that the effect of periodic boundary conditions is significant and cannot be ignored. Unfortunately, this former linear elastic theory has been developed only for perfect dislocations. A similar theory for dissociated dislocations is not available, but is critical for researchers to explain the dissociation energy, stacking fault width, and the consequent deformation phenomena observed in simulations.

Concerning an infinite dislocation array, the total elastic energy involved is an infinite sum. Some previous studies performed this summation numerically, where a conditional divergence problem was reported and was dealt with using sophisticated algorithms.[2–4] Under the isotropic condition, we derived a semi-analytical expression for the total elastic energy of the undissociated dislocation dipole array with fast convergence.[5,6] The purpose of this study is to extend our previous work[5,6] to include dissociated dislocations in isotropic materials. Semi-analytical expressions will be given for force, stacking fault width, and energy for dissociated dislocations and results will be discussed with reference to isolated dislocations.

Mechanics of Materials Department, Sandia National Laboratories, Livermore, California 94550, USA. E-mail: xzhou@sandia.gov

2. Forces between partials

(A) Analytical expression for force

The simplest dislocations that can be simulated under the periodic boundary conditions are dislocation dipoles. Geometries of our three-dimensional periodic dislocation dipoles are illustrated in Fig. 1, where the orange frames highlight the unit cell at the origin $i, j = 0, 0$ whose dimensions in x and y directions are respectively L_x and L_y. Under the periodic boundary conditions, such a unit cell can be viewed as being infinitely repeated in space $i, j = -\infty, \ldots, +\infty$. Each cell contains one dislocation dipole whose separation distance is d. In Fig. 1(a), dislocations are undissociated and the two dislocations of the dipole in each cell are marked as $\alpha_{i,j}$ and $\alpha'_{i,j}$ respectively. In Fig. 1(b), the dislocation $\alpha_{i,j}$ is dissociated into two partials $a_{i,j}$ and $b_{i,j}$, and the dislocation $\alpha'_{i,j}$ is dissociated into two partials $a'_{i,j}$ and $b'_{i,j}$. To clearly distinguish the two arrays of partials, one is coloured black and the other one is coloured blue.

The stacking fault width λ shown in Fig. 1(b) is a technologically important property. To understand λ, the x component of the force between the black and blue partial dislocations needs to be understood. In a per dislocation unit, this force can be calculated as the total x-component force between a chosen

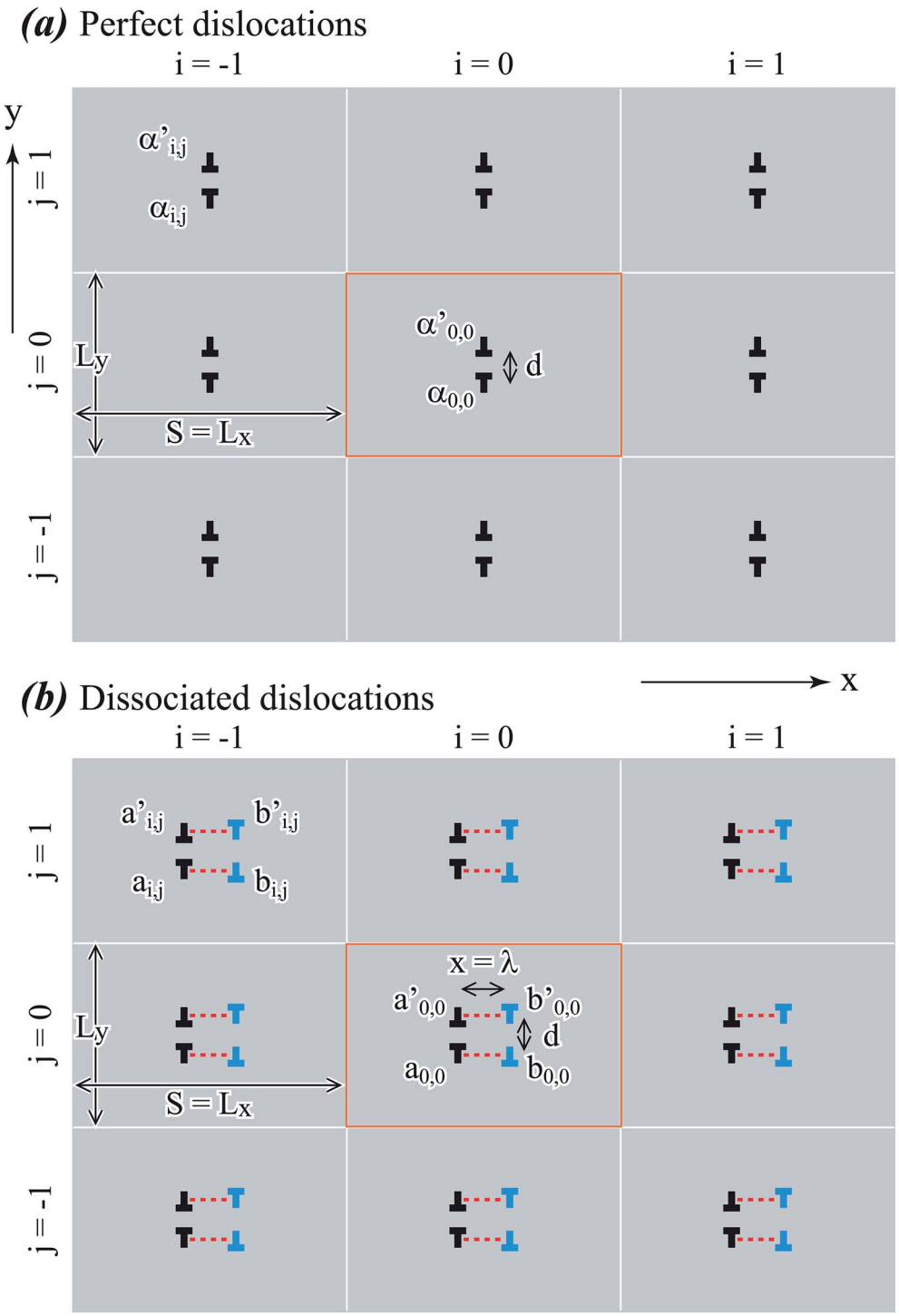

Fig. 1 Geometries for periodic dislocation dipole arrays: (a) perfect dislocations and (b) dissociated dislocations.

blue dislocation (say, $b_{0,0}$) and all the black dislocations in the array. If the character angle and Burgers magnitude of the undissociated dislocation are β and b, the character angles of the two partials are $\beta + \pi/6$ and $\beta - \pi/6$ respectively, and both partials have the same Burgers magnitude of $b/\sqrt{3}$. When a blue dislocation is separated from the black dislocation by x and y in the horizontal and vertical directions, the black dislocation will apply an x-component force to the blue dislocation:[7]

$$f_x(x,y) = \frac{Gb^2(1-2\cos 2\beta)}{24\pi(1-\nu)}\frac{x(x^2-y^2)}{(x^2+y^2)^2} + \frac{Gb^2(1+2\cos 2\beta)}{24\pi}\frac{x}{x^2+y^2} \quad (1)$$

where G is the shear modulus and ν is Poisson's ratio. Now, we consider the interaction between the blue dislocation and any vertical column of black dislocations shown in Fig. 1(b). As will

be clear below, the column-by-column derivation of the interaction can eliminate the conditional divergence problem. Assume that the blue dislocation is horizontally separated from the black dislocation column by x_1, the dislocation column will apply a total x-component force $f_{x,\mathrm{col}}(x_1)$ to the blue dislocation. $f_{x,\mathrm{col}}(x_1)$ can be written as

$$f_{x,\mathrm{col}}(x_1) = \frac{Gb^2(1-2\cos 2\beta)}{24\pi(1-\nu)}c_{1\mathrm{e}} + \frac{Gb^2(1+2\cos 2\beta)}{24\pi}c_{1\mathrm{s}} \quad (2)$$

where functions $c_{1\mathrm{e}}(x_1)$ and $c_{1\mathrm{s}}(x_1)$ are expressed as

$$c_{1\mathrm{e}}(x_1) = \frac{1}{x_1} - \frac{x_1\left({x_1}^2 - d^2\right)}{\left({x_1}^2 + d^2\right)^2} + \sum_{i=1}^{\infty}\left\{\frac{2x_1\left[{x_1}^2 - \left(iL_y\right)^2\right]}{\left[{x_1}^2 + \left(iL_y\right)^2\right]^2} - \frac{x_1\left[{x_1}^2 - \left(iL_y - d\right)^2\right]}{\left[{x_1}^2 + \left(iL_y - d\right)^2\right]^2} - \frac{x_1\left[{x_1}^2 - \left(iL_y + d\right)^2\right]}{\left[{x_1}^2 + \left(iL_y + d\right)^2\right]^2}\right\} \quad (3)$$

$$c_{1\mathrm{s}}(x_1) = \frac{1}{x_1} - \frac{x_1}{{x_1}^2 + d^2} + \sum_{i=1}^{\infty}\left(\frac{2x_1}{{x_1}^2 + \left(iL_y\right)^2} - \frac{x_1}{{x_1}^2 + \left(iL_y - d\right)^2} - \frac{x_1}{{x_1}^2 + \left(iL_y + d\right)^2}\right) \quad (4)$$

Eqn (3) and (4) essentially sum up the interaction between the blue dislocation and the dislocations in the column in the sequence of their separation distances in y: 0, d, L_y, L_y, $L_y - d$, $L_y + d$, $2L_y$, $2L_y$, $2L_y - d$, $2L_y + d$, …, this sequence is followed to ensure convergence. For instance, it will have a conditional divergence problem if $\sum_{i=1}^{\infty}\left[\frac{2x_1}{{x_1}^2 + (iL_y)^2} - \frac{x_1}{{x_1}^2 + (iL_y - d)^2} - \frac{x_1}{{x_1}^2 + (iL_y + d)^2}\right]$ is written as $\sum_{i=1}^{\infty}\frac{2x_1}{{x_1}^2 + (iL_y)^2} - \sum_{i=1}^{\infty}\frac{x_1}{{x_1}^2 + (iL_y - d)^2} - \sum_{i=1}^{\infty}\frac{x_1}{{x_1}^2 + (iL_y + d)^2}$. The infinite summations in eqn (3) and (4) have closed-form solutions written as follows:

$$c_{1\mathrm{e}}(x_1) = \frac{\pi^2 x_1}{{L_y}^2}\left\{\left[\mathrm{csch}\left(\frac{\pi x_1}{L_y}\right)\right]^2 - \frac{4\exp\left(\frac{2\pi x_1}{L_y}\right)\left[-2\exp\left(\frac{2\pi x_1}{L_y}\right) + \cos\left(\frac{2d\pi}{L_y}\right) + \exp\left(\frac{4\pi x_1}{L_y}\right)\cos\left(\frac{2d\pi}{L_y}\right)\right]}{\left[1 + \exp\left(\frac{4\pi x_1}{L_y}\right) - 2\exp\left(\frac{2\pi x_1}{L_y}\right)\cos\left(\frac{2d\pi}{L_y}\right)\right]^2}\right\} \quad (5)$$

$$c_{1\mathrm{s}}(x_1) = \frac{2\pi}{L_y}\frac{\coth\left(\frac{\pi x_1}{L_y}\right)\left[\sin\left(\frac{d\pi}{L_y}\right)\right]^2}{\cosh\left(\frac{2\pi x_1}{L_y}\right) - \cos\left(\frac{2d\pi}{L_y}\right)} \quad (6)$$

where csch(), coth(), and cosh() are the hyperbolic cosecant, cotangent, and cosine functions respectively. Obtaining the closed-form solution for eqn (3) and (4) eliminates the conditional divergence problem. The force $f_{x,\mathrm{array}}(x)$ applied by the entire black dislocation array to the blue dislocation can be expressed as a function of partial separation distance x. $f_{x,\mathrm{array}}(x)$ can be obtained similarly as follows:

$$f_{x,\mathrm{array}}(x) = \frac{Gb^2(1-2\cos 2\beta)}{24\pi(1-\nu)}c_{2\mathrm{e}} + \frac{Gb^2(1+2\cos 2\beta)}{24\pi}c_{2\mathrm{s}} \quad (7)$$

where functions $c_{2\mathrm{e}}$ and $c_{2\mathrm{s}}$ are expressed as follows:

$$c_{2\mathrm{e}}(x) = c_{1\mathrm{e}}(x) + \sum_{i=1}^{\infty}[c_{1\mathrm{e}}(j \times L_x + x) - c_{1\mathrm{e}}(j \times L_x - x)] \quad (8)$$

$$c_{2\mathrm{s}}(x) = c_{1\mathrm{s}}(x) + \sum_{i=1}^{\infty}[c_{1\mathrm{s}}(j \times L_x + x) - c_{1\mathrm{s}}(j \times L_x - x)] \quad (9)$$

Eqn (8) and (9) essentially sum up the interaction between the blue dislocation and the black dislocation columns in the sequence of column location $x_1 = x$, $L_x + x$, $L_x - x$, $2L_x + x$, $2L_x - x$, …. We cannot find closed-form solutions for eqn (8) and (9). This is not important because eqn (8) and (9) converge rapidly. We can illustrate this by examining the convergence curves of $c_{2\mathrm{e}}$ and $c_{2\mathrm{s}}$ as a function of number of summation terms N. We note that eqn (8) and (9) involve four parameters L_x, L_y, d, and x, so Fig. 2(a)–(d) show the convergence curves at four representative sets of parameters (L_x, L_y, d, and x). Here, we fix $L_y = 2d$ because this gives a maximum dislocation dipole energy,[5,6] and fix L_y = 420 Å because from eqn (5)–(9), the convergence depends primarily on L_x/L_y (note $x_1 = j \times L_x + x$, j = 1, 2, …), so that we only need to explore the L_x effect at a given L_y. Physically, a large L_x means that the next column is farther away, and a small L_y means that opposite elastic fields of dislocation dipoles along the y direction cancel more quickly.

Fig. 2 confirms that eqn (8) and (9) converge extremely fast especially for large L_x values. For instance, at L_x = 2100 Å (Fig. 2(d)), convergence is achieved without any summation terms. Convergence is relatively slower at smaller L_x, but even at L_x = 20 Å which is below the dimension used in most atomistic simulations, the convergence is still well achieved with about 25 summation terms. Interestingly, unlike the isolated dislocation where $c_{2\mathrm{e}}(x) = c_{2\mathrm{s}}(x) = 1/x$, $c_{2\mathrm{e}}(x)$ and $c_{2\mathrm{s}}(x)$ under the periodic boundary conditions are in some cases not equal. They can also differ significantly from the isolated dislocation case, meaning that the effect of the periodic boundary conditions on dislocation dissociation cannot be ignored. For the cases we tested,

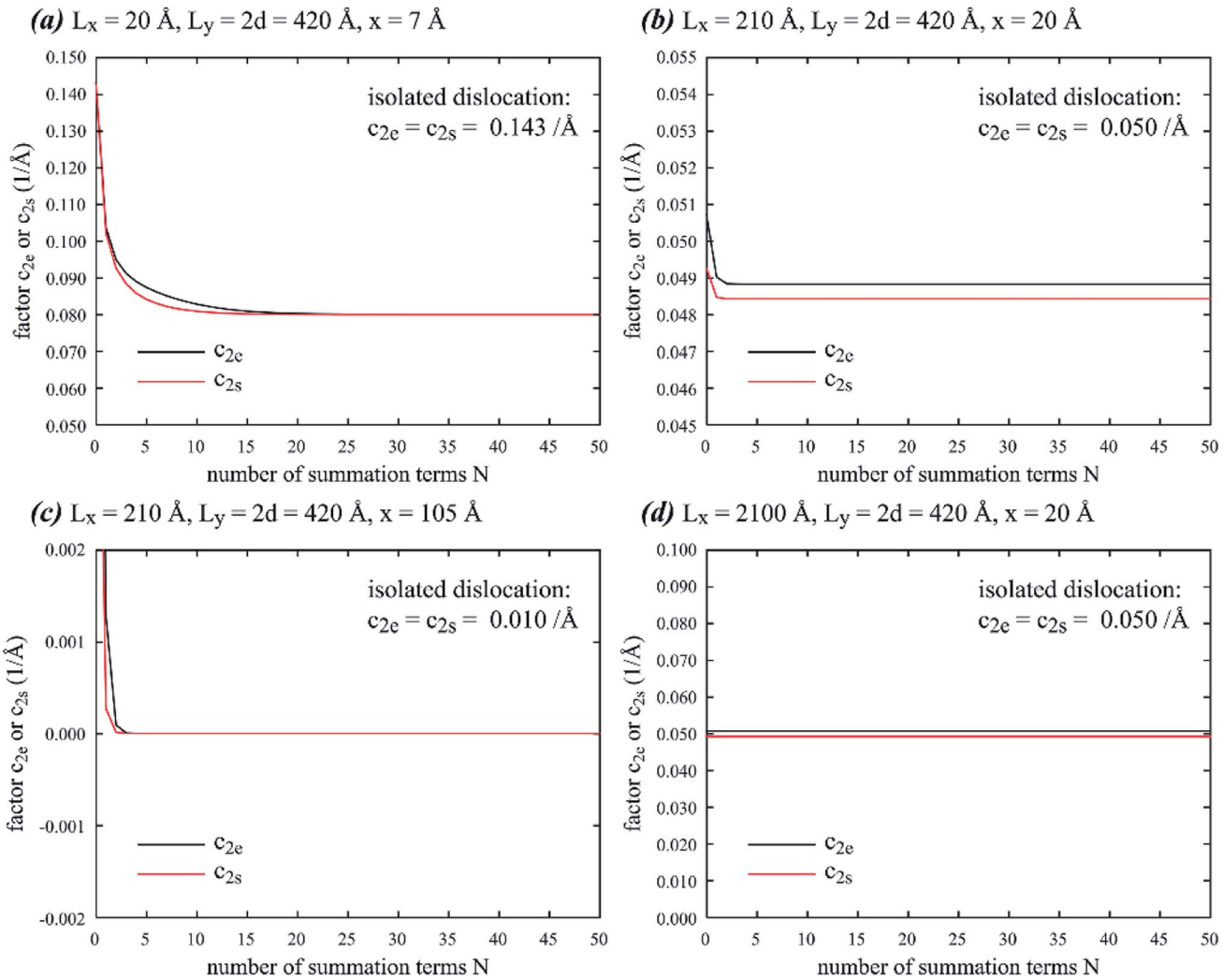

Fig. 2 Factors c_{2e} and c_{2s} as a function of summation number N at four different sets of geometric parameters: (a) $L_x = 20$ Å, $L_y = 2d = 420$ Å, $x = 7$ Å, (b) $L_x = 210$ Å, $L_y = 2d = 420$ Å, $x = 20$ Å, (c) $L_x = 210$ Å, $L_y = 2d = 420$ Å, $x = 105$ Å, and (d) $L_x = 2100$ Å, $L_y = 2d = 420$ Å, $x = 20$ Å.

only when periodic length L_x and L_y are both large and the partial separation distance x is small (Fig. 2(d)), will $c_{2e}(x)$ and $c_{2s}(x)$ both approach the value for isolated dislocation.

In the following calculations, we will use summation number $N = 100$, which will ensure convergence according to Fig. 2.

(B) Comparison of force with isolated dislocation

Eqn (7) indicates that the force between partials is determined by functions $c_{2e}(x)$ and $c_{2s}(x)$. Hence, comparison of force between periodic partials and isolated pairs of partials can be achieved by comparing $c_{2e}(x)$ and $c_{2s}(x)$, which, for isolated partials, satisfy $c_{2e}(x) = c_{2s}(x) = 1/x$. Fig. 3 compares results from periodic and isolated partials on factors $c_{2e}(x)$ and $c_{2s}(x)$ as a function of partial separation distance x at different dipole lengths d, and x and y dimensions L_x and L_y: (a) $d = 15$ and 150 Å, $L_x = 200$ Å, $L_y = 300$ Å; (b) $d = 1$ and 10 Å, $L_x = 200$ Å, $L_y = 20$ Å; (c) $d = 15$ and 150 Å, $L_x = 20$ Å, $L_y = 300$ Å; and (d) $d = 1$ and 10 Å, $L_x = 20$ Å, $L_y = 20$ Å. Fig. 3 indicates that when the plot range x spans the entire periodic length L_x, $c_{2e}(x)$ and $c_{2s}(x)$ are antisymmetric at $x = L_x/2$ where force would drop to zero ($c_{2e} = c_{2s} = 0$). This is a validation of the results because from Fig. 1(b), any partial dislocation, say, $b_{0,0}$, would be subject to equal forces from neighbouring partials, say $a_{0,0}$ and $a_{1,0}$, in opposite directions when $x = L_x/2$. As a result, zero force would be achieved at the antisymmetric middle point $x = L_x/2$. Because $c_{2e}(x)$ and $c_{2s}(x)$ always drop to zero at $x = L_x/2$ while the function $1/x$ does not have this feature, Fig. 3 confirms that the force between periodic partials is significantly different from that between isolated partials when x approaches $L_x/2$. However, when $x \ll L_x/2$, the force between periodic partials can be quite close to that between isolated partials if the dipole length d is large enough. The exception is when d is small, where $c_{2e}(x)$ and $c_{2s}(x)$ are significantly lower than $1/x$. This is because the dislocation dipole increasingly annihilates when d reduces. Like Fig. 2, Fig. 3 also shows that $c_{2e}(x)$ and $c_{2s}(x)$ can be different in some cases.

(C) Stacking fault width

Stacking fault width λ results from the balance between dislocation force $f_{x,\text{array}}$ and stacking fault energy force γ, and it can therefore be solved from

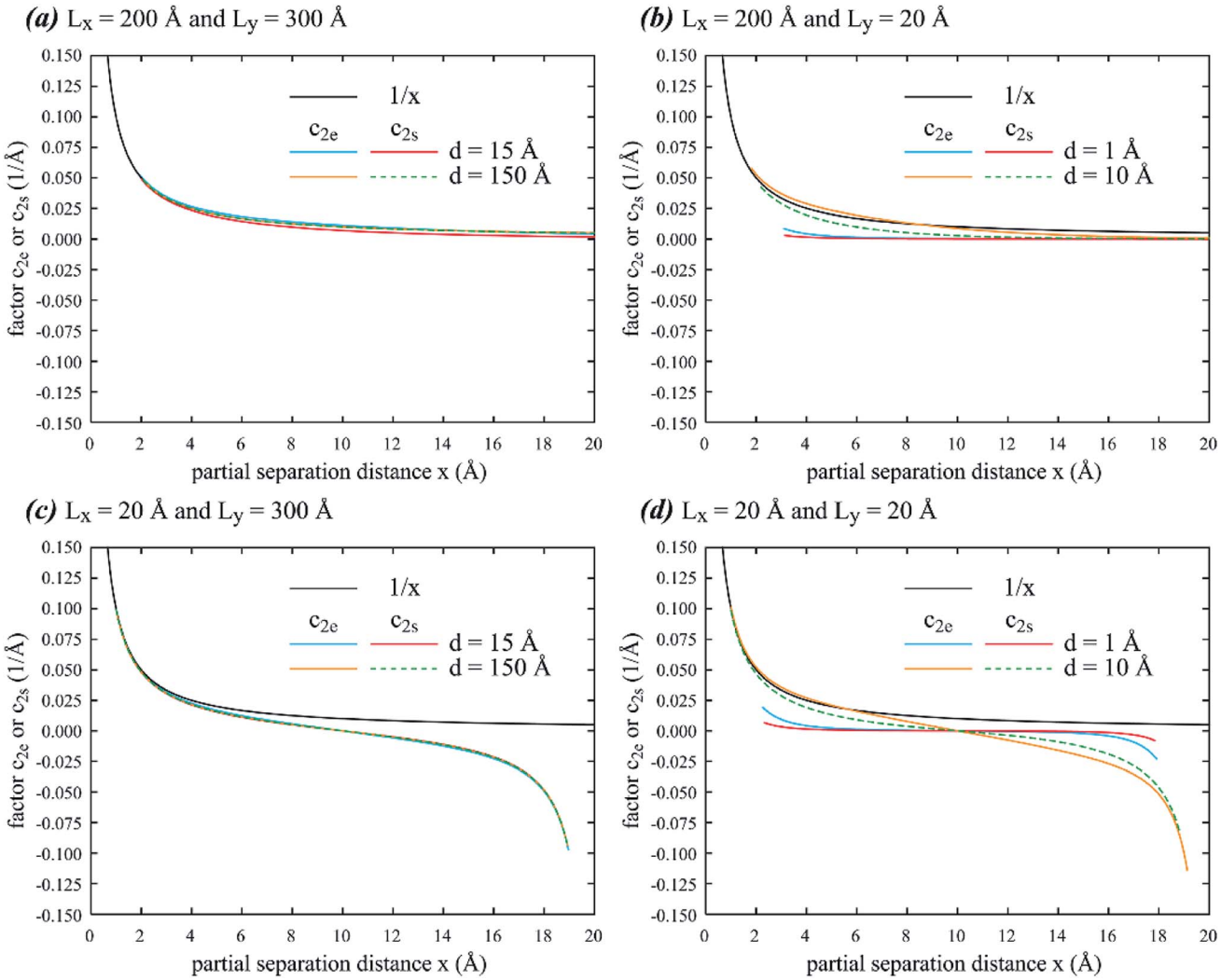

Fig. 3 Factors c_{2e} and c_{2s} as a function of partial separation distance x at different dipole lengths d, and x and y dimensions L_x and L_y: (a) $d = 15$ and 150 Å, $L_x = 200$ Å, $L_y = 300$ Å; (b) $d = 1$ and 10 Å, $L_x = 200$ Å, $L_y = 20$ Å; (c) $d = 15$ and 150 Å, $L_x = 20$ Å, $L_y = 300$ Å; and (d) $d = 1$ and 10 Å, $L_x = 20$ Å, $L_y = 20$ Å.

$$f_{x,\text{array}}(\lambda) = \gamma \tag{10}$$

For isolated dislocation, stacking fault width is

$$\lambda = \frac{Gb^2(1 - 2\cos 2\beta)}{24\pi\gamma(1-\nu)} + \frac{Gb^2(1 + 2\cos 2\beta)}{24\pi\gamma} \tag{11}$$

We now compare stacking fault width of periodic and isolated partials using parameters derived from an aluminum interatomic potential:[5,8] $G = 0.1830$ eV Å^{-3}, $\nu = 0.3874$, $b = 2.864$ Å, and $\gamma = 0.0083$ eV Å^{-2}. Fig. 4(a) and (b) show, respectively, stacking fault width λ of edge and screw dislocations as a function of L_x at different combinations of L_y and d, where the λ value from isolated dislocation is marked by the dashed line.

Fig. 4 indicates that stacking fault width λ is narrower for screw dislocation than for edge dislocation, and λ is sensitive to cell dimensions. When L_x, L_y, and d are all large, λ approaches the value for isolated dislocation as expected. When L_x is small, λ is small as it is limited by $L_x/2$. The sensitivity to L_x reduces when L_x increases, but the saturated λ still depends on L_y, d, and the dislocation type. Normally, it can be thought that the periodic boundary conditions would constrain dislocations. It is therefore surprising that for the edge dislocation, λ is larger than the value from isolated dislocation at relatively small values of $L_y = 40$ Å and $d = 20$ Å. This phenomenon is not observed for the screw dislocation results in Fig. 4(b). The complex relationships between λ and computational geometry present a warning to our past interpretations of dislocation dissociation under the periodic boundary conditions.

(D) Molecular dynamics validation of stacking fault width

Selected atomistic simulations are performed to validate the stacking fault width calculations. The methods developed previously[5] are used to introduce dislocation dipoles in atomistic systems. Using the same aluminum interatomic potential as that used previously,[5,8] and applying a zero-pressure NPT

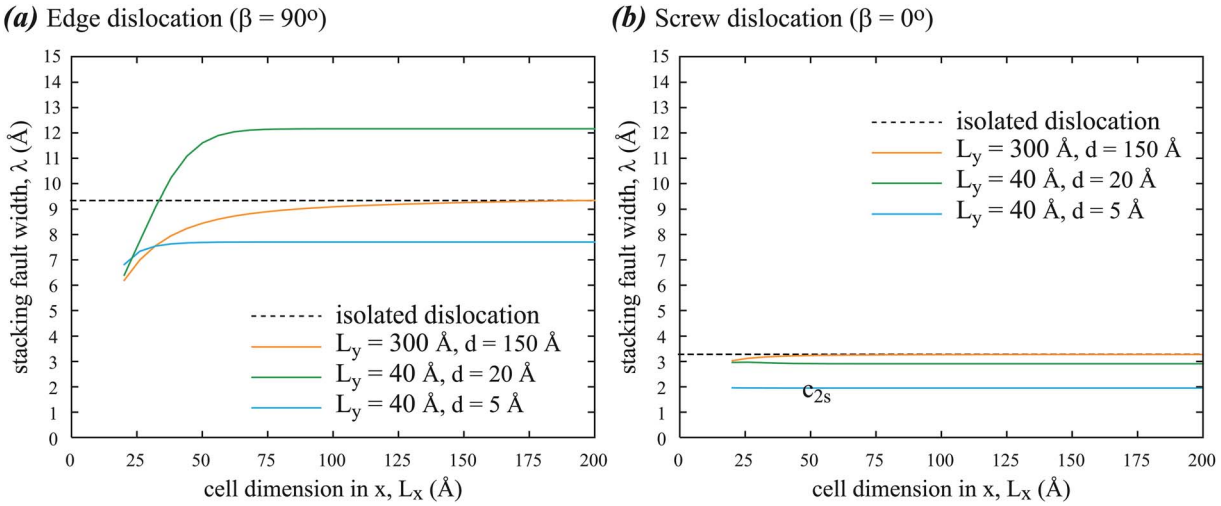

Fig. 4 Stacking fault width λ of (a) edge and (b) screw dislocations as a function of x dimension L_x at different y dimensions and dipole lengths, L_y and d.

ensemble (*i.e.*, number of atoms, pressure, and temperature are kept constant) with the periodic boundary conditions, molecular dynamics (MD) simulations are performed for 4 ns at 300 K. The structures are further relaxed using energy minimization. To ensure that dislocation does not randomly migrate during the MD simulations, the centre of mass of small regions above and below the dislocations is not allowed to shift. Four consecutive (111) planes near an edge and a screw dislocation, obtained from simulations at different L_x and L_y (d is taken at L_y/2), are shown in Fig. 5(a) and (b), where different colours indicate OVITO results of local structures (fcc for face-centred-cubic, hcp for hexagonally closely packed, and bcc for body centred cubic).[9,10] Fig. 5(a) confirms that in the edge dislocation case, the stacking fault width at $L_x \sim 40$ Å is narrower than that at $L_x \sim 200$ Å, and the magnitudes of both widths are quite close to those shown in Fig. 4(a). Fig. 5(b) shows no hcp atoms that typically occur within the stacking faults. This means that the stacking fault width of the screw dislocation is narrower than that of the edge dislocation, which is also consistent with Fig. 4.

Aluminum has an fcc structure. Atomistic simulations are also performed for bcc tungsten using the embedded-atom method potential.[11] Two consecutive (110) planes near an edge dislocation obtained from simulations at $L_x = 66$ Å and $L_y = 403$ Å and two different values of $d = 22$ and 112 Å are included in Fig. 5(c). Following the previous approach,[5] we found that this potential gives lattice constant $a = 3.1686$ Å and shear modulus $G = 1.0016$ eV Å^{-3} at a chosen Poisson's ratio of $\nu = 0.3$. Experiments indicated that tungsten has a stacking fault energy of $\gamma = 0.03$ eV Å^{-2}.[12] Based on these parameters, eqn (10) would give $\lambda = \sim$10–13 Å for the two cases shown in Fig. 5(c), which seems to be in good agreement.

3. Dislocation energies

(A) Previous works on dislocation energy

According to the previous works,[5,6] the per unit length energy Γ for periodic dislocation arrays can be expressed as follows:

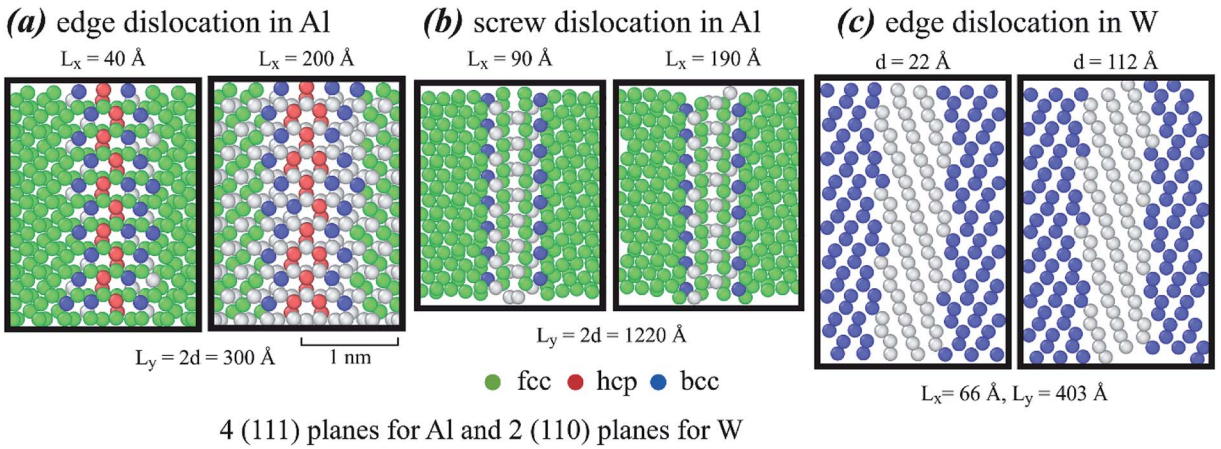

Fig. 5 Dislocation configurations obtained from atomistic simulations for (a) edge dislocation in aluminum, (b) screw dislocation in aluminum, and (c) edge dislocation in tungsten.

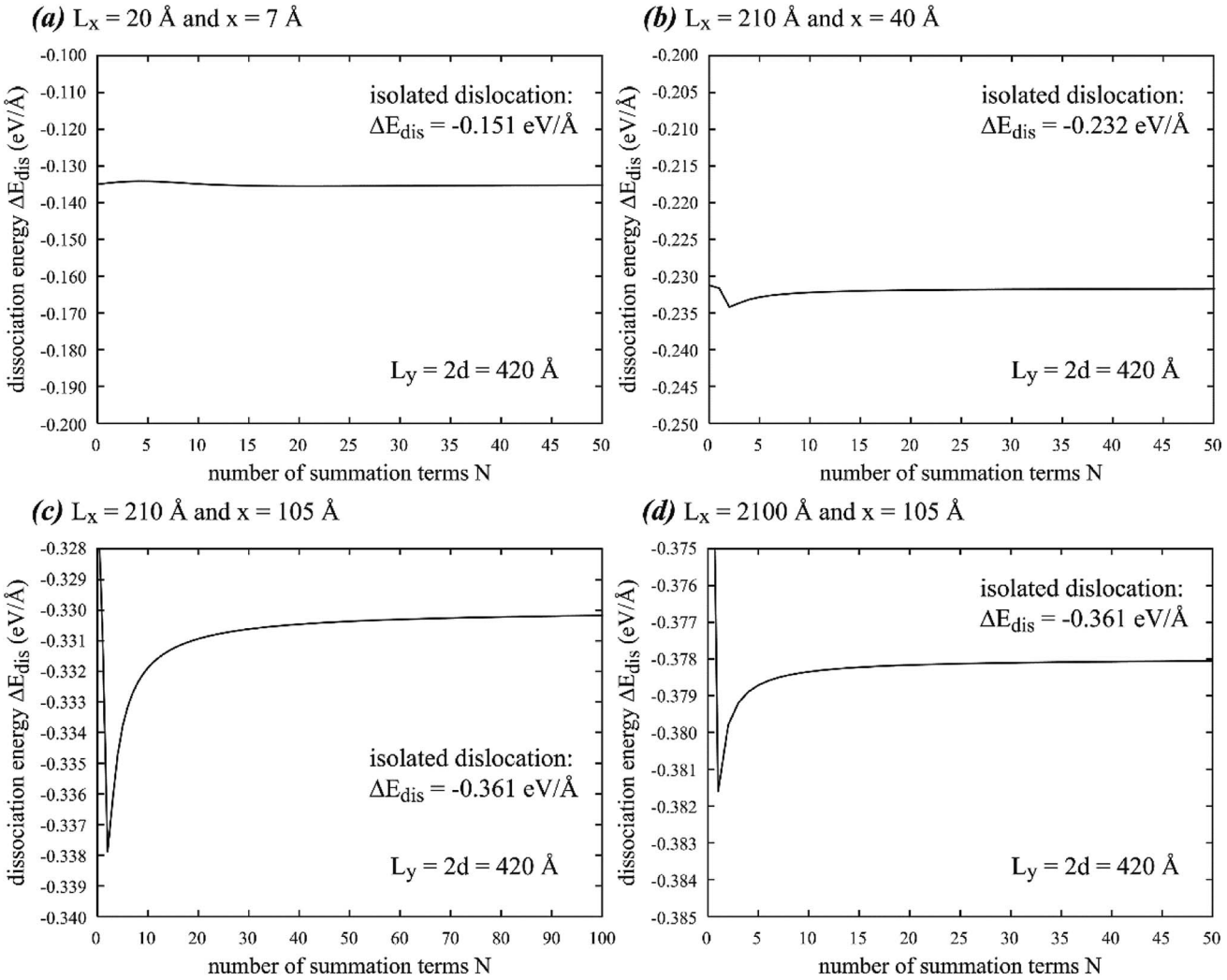

Fig. 6 Dissociation energy ΔE_{dis} as a function of number of summation terms N at fixed y dimension $L_y = 420$ Å, dipole length $d = 210$ Å, and four different sets of x dimension L_x and partial spacing x of (a) $L_x = 20$ Å, $x = 7$ Å, (b) $L_x = 210$ Å, $x = 40$ Å, (c) $L_x = 210$ Å, $x = 105$ Å, and (d) $L_x = 2100$ Å, $x = 105$ Å. Note that results from periodic and isolated dislocations may differ.

$$\Gamma = E_c + \frac{Gb^2 \sin^2\beta}{4\pi(1-\nu)} \ln\frac{1}{r_0} + \frac{Gb^2 \sin^2\beta}{4\pi(1-\nu)}[c_{ue0}(d) + c_{ue}(d)] + \frac{Gb^2 \cos^2\beta}{4\pi} \ln\frac{1}{r_0} + \frac{Gb^2 \cos^2\beta}{4\pi}[c_{us0}(d) + c_{us}(d)] + \Delta E_{dis} \tag{12}$$

where E_c and r_0 are the core energy and core radius respectively, ΔE_{dis} is the dissociation energy per unit length, and functions $c_{ue0}(d)$, $c_{us0}(d)$, $c_{ue}(d)$, $c_{us}(d)$ are expressed as follows:

$$c_{ue0}(d) = \ln\left[\frac{(L_y - d)d}{L_y}\right] - \ln\left[Ga\left(\frac{L_y + d}{L_y}\right)\right] - \ln\left[Ga\left(2 - \frac{d}{L_y}\right)\right] \tag{13}$$

$$c_{us0}(d) = \ln\left[\frac{(L_y - d)d}{L_y}\right] - \ln\left[Ga\left(\frac{L_y + d}{L_y}\right)\right] - \ln\left[Ga\left(2 - \frac{d}{L_y}\right)\right] \tag{14}$$

$$c_{ue}(d) = \sum_{i=1}^{\infty}\left\{\frac{4\pi \times i \times L_x \times \coth\left(\frac{\pi \times i \times L_x}{L_y}\right)\sin^2\left(\frac{\pi d}{L_y}\right)}{L_y \cosh\left(\frac{2\pi \times i \times L_x}{L_y}\right) - L_y \times \cos\left(\frac{2\pi d}{L_y}\right)} + \ln\left[\cos^2\left(\frac{\pi d}{L_y}\right) + \coth^2\left(\frac{\pi \times i \times L_x}{L_y}\right)\sin^2\left(\frac{\pi d}{L_y}\right)\right]\right\} \tag{15}$$

$$c_{us}(d) = \sum_{i=1}^{\infty}\ln\left[\cos^2\left(\frac{\pi d}{L_y}\right) + \coth^2\left(\frac{\pi \times i \times L_x}{L_y}\right)\sin^2\left(\frac{\pi d}{L_y}\right)\right] \tag{16}$$

Like eqn (8), (9), (15) and (16) also converge rapidly, so that our choice of 100 summation terms is enough to ensure accurate results.[5] The past works[1–5] have not addressed the dissociation energy ΔE_{dis}, which is the focus of the following section.

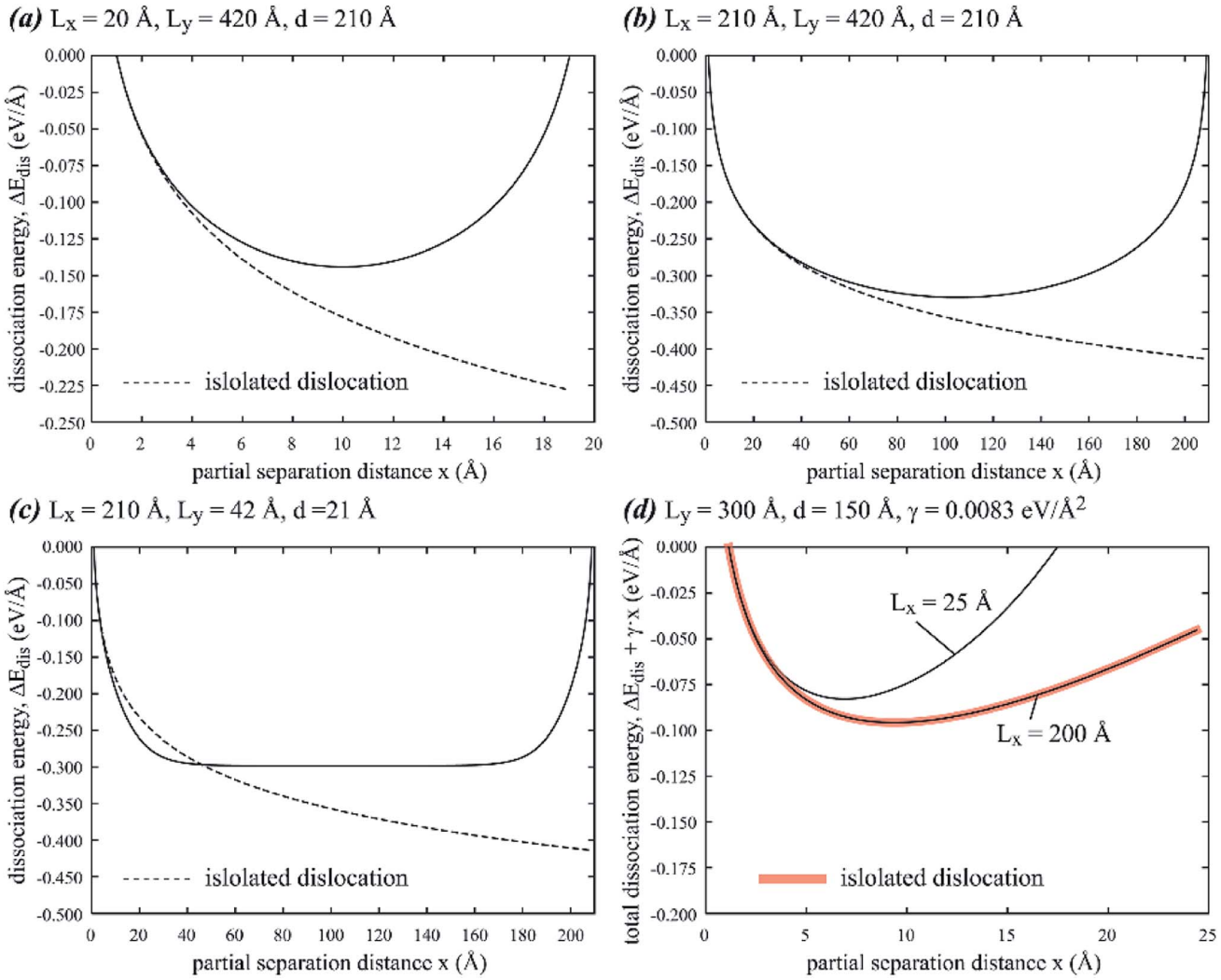

Fig. 7 Dissociation energy ΔE_{dis} as a function of partial spacing x for (a) $L_x = 20$ Å, $L_y = 420$ Å, $d = 210$ Å, (b) $L_x = 210$ Å, $L_y = 420$ Å, $d = 210$ Å, and (c) $L_x = 210$ Å, $L_y = 42$ Å, $d = 21$ Å. Total dissociation energy $\Delta E_{dis} + \gamma x$ as a function of x for (d) $L_y = 300$ Å, $d = 150$ Å, $\gamma = 0.0083$ eV Å^{-2} and two different values $L_x = 25$ Å and $L_x = 250$ Å.

(B) Analytical expression for ΔE_{dis}

Direct integration of stress and strain fields of all partials is challenging. Alternatively, dissociation energy ΔE_{dis} can be calculated based on the work done when the blue dislocations in Fig. 1(b) are displaced from an initial location $x = 0$ to a final location $x = \lambda$. To avoid singularity at $x = 0$, we will derive the work from an initial location $x = L_x/2$ instead. This does not change the relative energy, but changes only the reference state from $x = 0$ to $x = L_x/2$.

In a per dislocation unit, we only consider the work done between a chosen blue dislocation (say, $b_{0,0}$) and all the black dislocations in array. To displace any pair of blue and black dislocations from an initial x-spacing x_1 to a final x-spacing x_2 without changing the y-spacing y, the work done is $w(x_1, x_2, y) = \int_{x_1}^{x_2} f_x(x, y)$. Using eqn (1), we have the following:

$$w(x_1, x_2, y) = \frac{Gb^2[1 - 2\cos(2\beta)]}{48\pi(1-\nu)}\left\{\ln\left[\frac{x_2^2 + y^2}{x_1^2 + y^2}\right] + \frac{2y^2}{x_2^2 + y^2} - \frac{2y^2}{x_1^2 + y^2}\right\} + \frac{Gb^2[1 + 2\cos(2\beta)]}{48\pi}\ln\left[\frac{x_2^2 + y^2}{x_1^2 + y^2}\right] \quad (17)$$

We first calculate the total work done by the black dislocation row at $y = 0$ due to the displacement from $x = L_x/2$ to $x = x$. This work can be written as follows:

$$w_{row}(x, y = 0) = \frac{Gb^2[1 - 2\cos(2\beta)]}{48\pi(1-\nu)} c_{e0}(x) + \frac{Gb^2[1 + 2\cos(2\beta)]}{48\pi} c_{s0}(x) \quad (18)$$

where

$$c_{e0}(x) = c_{s0}(x) = 2\ln\prod_{i=1}^{\infty}\left[\frac{(i-1)L_x + x}{(i-1)L_x + L_x/2} \times \frac{-i\times L_x + x}{-i\times L_x + L_x/2}\right] = \ln\left[\sin^2\left(\frac{\pi x}{L_x}\right)\right] \tag{19}$$

Note that eqn (19) essentially sums up $\ln({x_2}^2/{x_1}^2)$ in a sequence of $x_1 = (i-1)\times L_x + L_x/2$, $x_2 = (i-1)\times L_x + x$, and $x_1 = -i\times L_x + L_x/2$, $x_2 = -i\times L_x + x$ ($i = 1, 2, \ldots$), and it has a closed-form solution. Next, we calculate the total work done by any vertical column of black dislocations (except the dislocation at $y = 0$). Assuming that the initial and final x-spacings between the blue dislocation and the black dislocation column are x_1 and x_2 respectively, this work can be written as follows:

$$w_{col}(x_1, x_2, y\neq 0) = \frac{Gb^2[1-2\cos(2\beta)]}{48\pi(1-\nu)}[c_{3e,1}(x_1,x_2) + c_{3e,2}(x_1,x_2)] + \frac{Gb^2[1+2\cos(2\beta)]}{48\pi}c_{3s}(x_1,x_2) \tag{20}$$

By summing up eqn (17) in the similar y sequence as described above, we can find:

$$c_{3e,1}(x_1,x_2) = c_{3s}(x_1,x_2) = \ln\left(\frac{d^2+{x_1}^2}{d^2+{x_2}^2}\right) + \ln\prod_{i=1}^{\infty}\left[\frac{{x_2}^2+(i\times L_y)^2}{{x_1}^2+(i\times L_y)^2} \times \frac{{x_1}^2+(i\times L_y - d)^2}{{x_2}^2+(i\times L_y - d)^2} \times \frac{{x_2}^2+(i\times L_y)^2}{{x_1}^2+(i\times L_y)^2} \times \frac{{x_1}^2+(i\times L_y + d)^2}{{x_2}^2+(i\times L_y + d)^2}\right] \tag{21}$$

$$c_{3e,2}(x_1,x_2) = \frac{2d^2}{d^2+{x_1}^2} - \frac{2d^2}{d^2+{x_2}^2} + \sum_{i=1}^{\infty}\left[-\frac{4(i\times L_y)^2}{{x_1}^2+(i\times L_y)^2} + \frac{2(i\times L_y - d)^2}{{x_1}^2+(i\times L_y - d)^2} + \frac{2(i\times L_y + d)^2}{{x_1}^2+(i\times L_y + d)^2} + \frac{4(i\times L_y)^2}{{x_2}^2+(i\times L_y)^2} - \frac{2(i\times L_y - d)^2}{{x_2}^2+(i\times L_y - d)^2} - \frac{2(i\times L_y + d)^2}{{x_2}^2+(i\times L_y + d)^2}\right] \tag{22}$$

Eqn (21) and (22) have a closed-form solution:

$$c_{3e,1}(x_1,x_2) = c_{3s}(x_1,x_2) = \ln\left(\frac{{x_1}^2}{2{x_2}^2}\right) + \ln\left[2\,\mathrm{csch}^2\left(\frac{\pi x_1}{L_y}\right)\sinh^2\left(\frac{\pi x_2}{L_y}\right)\frac{\cos\left(\frac{2\pi d}{L_y}\right) - \cosh\left(\frac{2\pi x_1}{L_y}\right)}{\cos\left(\frac{2\pi d}{L_y}\right) - \cosh\left(\frac{2\pi x_2}{L_y}\right)}\right] \tag{23}$$

$$c_{3e,2}(x_1,x_2) = \frac{2\pi x_1}{L_y}\coth\left(\frac{\pi x_1}{L_y}\right) + \frac{4\pi x_2}{L_y}\frac{\coth\left(\frac{\pi x_2}{L_y}\right)\sin^2\left(\frac{\pi d}{L_y}\right)}{\cos\left(\frac{2\pi d}{L_y}\right) - \cosh\left(\frac{2\pi x_2}{L_y}\right)} + \frac{2\pi x_1}{L_y}\frac{\sinh\left(\frac{2\pi x_1}{L_y}\right)}{\cos\left(\frac{2\pi d}{L_y}\right) - \cosh\left(\frac{2\pi x_1}{L_y}\right)} \tag{24}$$

The total work done by the entire black dislocation arrays, from initial partial separation distance $L_x/2$ to final separation distance x, can be expressed as follows:

$$w(x) = w_{row}(x, y=0) + \sum_{i=1}^{\infty}\left\{w_{col}[(i-1)\times L_x + L_x/2, (i-1)\times L_x + x, y\neq 0] + w_{col}\left[-i\times L_x + \frac{L_x}{2}, -i\times L_x + x, y\neq 0\right]\right\} \tag{25}$$

Again, the summation in eqn (25) follows a similar sequence described above. Considering that energy has an opposite sign to work, and that the reference state of dissociation energy is undissociated dislocation (*i.e.*, $x = 0$ rather than $L_x/2$), the dissociation energy as a function of partial separation distance x can then be simply expressed as follows:

$$\Delta E_{dis}(x) = -[w(x) - w(r_0)] \tag{26}$$

Note that to avoid singularity, our reference state is taken as $x = r_0$ rather than $x = 0$, where r_0 is the dislocation core radius. Eqn (18)–(20) and (23)–(26) can be conveniently used to calculate the dissociation energy.

Since eqn (25) is not a closed form, we first explore its convergence. Based on the aluminum parameters cited above, $\Delta E_{dis}(x)$ is calculated as a function of the number of summation terms N at fixed $L_y = 2d = 420$ Å, and the results are shown in Fig. 6(a)–(d) for four different sets of L_x and x. It can be seen that while the convergence rate increases when L_x is increased and x is decreased, the effect of x becomes more significant. Given that $L_y = 2d = 420$ Å, accurate results can be achieved without any summation terms in Fig. 6(a) at the small partial spacing $x = 7$ Å, despite that $L_x = 20$ Å is also small. If L_x is not too large,

say 210 Å, and x is large, say 107 Å (the maximum x for a given L_x is $L_x/2$), then accurate results may require ~100 summation terms, as shown in Fig. 6(c). Such a large partial spacing (or under the equilibrium condition, the stacking fault width), however, is unlikely to be encountered.

The effect of x is a new finding as we have not thoroughly explored this in Fig. 2. Regardless, Fig. 6 confirms that our use of $N = 100$ is still extremely conservative for any practical stacking fault width.

(C) Comparison of dissociation energy with isolated dislocation

With the convenient methods and the aluminum parameters discussed above, we calculate dissociation energy as a function of partial spacing x using three different sets of geometric parameters. The results of these calculations are shown in Fig. 7(a) for $L_x = 20$ Å, $L_y = 420$ Å, $d = 210$ Å, Fig. 7(b) for $L_x = 210$ Å, $L_y = 420$ Å, $d = 210$ Å, and Fig. 7(c) for $L_x = 210$ Å, $L_y = 42$ Å, $d = 21$ Å. Additionally, we also calculate total dissociation energy $\Delta E_{\text{dis}} + \gamma x$ as a function of x using fixed $L_y = 300$ Å, $d = 150$ Å, and two different L_x values of 25 Å and 200 Å, where $\gamma = 0.0083$ eV Å^{-2} is the stacking fault energy. The results of this calculation are shown in Fig. 7(d). The corresponding results from isolated dislocations are included as black dash lines in Fig. 7(a)–(c), and as a thick red line in Fig. 7(d).

Fig. 7 indicates the negative dissociation energy, confirming that dissociation is energetically favorable. ΔE_{dis} is symmetric with minimum at $x = L_x/2$, consistent with Fig. 3 that force drops to zero and is antisymmetric at $x = L_x/2$. Fig. 7 also indicates that ΔE_{dis} obtained from periodic and isolated dislocations deviate significantly at x near $L_x/2$ but can be quite close for small x. Interestingly, ΔE_{dis} for isolated dislocations can have both negative deviation as shown in Fig. 7(a) and (b) and positive deviation as shown in Fig. 7(c). The equilibrium stacking fault width, identified as $\lambda \sim 7$ Å at $L_x = 25$ Å and $\lambda \sim 9$ Å at $L_x = 200$ Å by the minimum energy point in Fig. 7(d), matches the corresponding results in Fig. 4. Interestingly, the $\Delta E_{\text{dis}} + \gamma x$ curve obtained for the cell parameters $L_y = 300$ Å, $d = 150$ Å, and $L_x = 200$ Å matches the corresponding curve from isolated dislocations at least for $x \leq 25$ Å. For this particular case, the stacking fault width from periodic boundary conditions matches that for isolated dislocations, which is also consistent with Fig. 4. This observation is useful to guide the choice of computational cell that facilitates the calculation of stacking fault energy from the measurement of stacking fault width in simulations. However, it should be noted that in this particular case, the energy minimum is not very sharp, meaning that the stacking fault width observed in atomistic simulations is likely to have a large uncertainty margin.

4. Conclusions

We have developed useful expressions to calculate the dissociation thermodynamics of periodic dislocation dipoles in isotropic materials. The results indicated that periodic boundary conditions have complex influences on partial dislocation interaction forces, stacking fault widths, and dissociation energies. Depending on the system dimensions and dipole length, stacking fault width under the periodic conditions can be both above and below the value obtained from isolated dislocations. We anticipate that our expressions will impact future atomistic studies of dislocation properties. As one particular case, the best current method to calculate the dislocation core energy is to fit the total dislocation energy obtained from atomistic simulations to continuum models using the periodic boundary conditions. Such continuum models have not accounted for dislocation dissociation effects. By considering dislocation dissociation, our new development will result in more accurate dislocation core energy calculations.

Conflicts of interest

There are no conflicts of interest to declare.

Acknowledgements

Sandia National Laboratories is a multi-mission laboratory managed and operated by National Technology and Engineering Solutions of Sandia, LLC, a wholly owned subsidiary of Honeywell International, Inc., for the U.S. Department of Energy's National Nuclear Security Administration under contract DE-NA-0003525. The authors gratefully acknowledge research support from the U.S. Department of Energy, Office of Energy Efficiency and Renewable Energy, Hydrogen and Fuel Cell Technologies Office. The views expressed in the article do not necessarily represent the views of the U.S. Department of Energy or the United States Government.

References

1 V. V. Bulatov and W. Cai, *Computer Simulations of Dislocations*, Oxford University Press, London, 2006.
2 W. Cai, V. V. Bulatov, J. Chang, J. Li and S. Yip, *Philos. Mag.*, 2003, **83**, 539.
3 W. Cai, V. V. Bulatov, J. Chang, J. Li and S. Yip, *Phys. Rev. Lett.*, 2001, **86**, 5727.
4 J. Li, C. Z. Wang, J. P. Chang, W. Cai, V. V. Bulatov, K. M. Ho and S. Yip, *Phys. Rev. B*, 2004, **70**, 104113.
5 X. W. Zhou, R. B. Sills, D. K. Ward and R. A. Karnesky, *Phys. Rev. B*, 2017, **95**, 054112.
6 X. W. Zhou, D. K. Ward, J. A. Zimmerman, J. L. Cruz-Campa, D. Zubia, J. E. Martin and F. van Swol, *J. Mech. Phys. Solids*, 2016, **91**, 265.
7 D. Hull and D. J. Bacon, *Introduction to dislocations*, Butterworth-Heinemann, Oxford, 4th edn, 2001.
8 X. W. Zhou, D. K. Ward and M. E. Foster, *J. Alloys Compd.*, 2016, **680**, 752.
9 A. Stukowski, *Modell. Simul. Mater. Sci. Eng.*, 2010, **18**, 015012.
10 A. Stukowski and K. Albe, *Modell. Simul. Mater. Sci. Eng.*, 2010, **18**, 085001.
11 X. W. Zhou, R. A. Johnson and H. N. G. Wadley, *Phys. Rev. B*, 2004, **69**, 144113.
12 B. Pegel, *Phys. Status Solidi*, 1968, **28**, 603.